







Article

Ratiometric Singlet Oxygen Sensor Based on BODIPY-DPA Dyad

Alexey A. Pakhomov ^{1,2,*}, Anastasia S. Belova ², Arevik G. Khchoyan ^{2,3}, Yuriy N. Kononevich ²,
Dmitriy S. Ionov ⁴, Margarita A. Maksimova ^{1,2,5}, Anastasiya Yu. Frolova ^{1,2}, Mikhail V. Alfimov ^{4,6},
Vladimir I. Martynov ¹ and Aziz M. Muzafarov ^{2,7}

- ¹ M.M. Shemyakin and Yu.A. Ovchinnikov Institute of Bioorganic Chemistry, Russian Academy of Sciences, 117997 Moscow, Russia
² A.N. Nesmeyanov Institute of Organoelement Compounds, Russian Academy of Sciences, 119991 Moscow, Russia
³ Faculty of Chemical-Pharmaceutical Technologies and Biomedical Preparations, Mendeleev University of Chemical Technology of Russia, 125047 Moscow, Russia
⁴ Photochemistry Center, FSRC “Crystallography and Photonics”, Russian Academy of Sciences, 119421 Moscow, Russia
⁵ Chemistry Department, M.V. Lomonosov Moscow State University, 119991 Moscow, Russia
⁶ Moscow Institute of Physics and Technology, State University, 141707 Dolgoprudny, Russia
⁷ N.S. Enikolopov Institute of Synthetic Polymeric Materials, Russian Academy of Sciences, 117393 Moscow, Russia
* Correspondence: alpah@mail.ru



Citation: Pakhomov, A.A.; Belova, A.S.; Khchoyan, A.G.; Kononevich, Y.N.; Ionov, D.S.; Maksimova, M.A.; Frolova, A.Y.; Alfimov, M.V.; Martynov, V.I.; Muzafarov, A.M. Ratiometric Singlet Oxygen Sensor Based on BODIPY-DPA Dyad. *Molecules* **2022**, *27*, 9060. <https://doi.org/10.3390/molecules27249060>

Academic Editors: Qi Sun and Jianguo Wang

Received: 5 December 2022

Accepted: 14 December 2022

Published: 19 December 2022

Publisher’s Note: MDPI stays neutral with regard to jurisdictional claims in published maps and institutional affiliations.



Copyright: © 2022 by the authors. Licensee MDPI, Basel, Switzerland. This article is an open access article distributed under the terms and conditions of the Creative Commons Attribution (CC BY) license (<https://creativecommons.org/licenses/by/4.0/>).

Abstract: Compounds sensitive to reactive oxygen species are widely used in the study of processes in living cells and in the development of therapeutic agents for photodynamic therapy. In the present work, we have synthesized a dyad in which the BODIPY dye is chemically bound to 9,10-diphenylanthracene (DPA). Here, DPA acts as a specific sensor of singlet oxygen and BODIPY as a reference dye. We studied the photophysical properties of the BODIPY-DPA dyad and showed that energy transfer occurs between the chromophores. As a result, the compound has excitation maxima in the absorption region of both DPA and BODIPY, but the fluorescence emission occurs mainly from BODIPY. In the presence of singlet oxygen, the excitation maximum of DPA decreases, while the intensity of the excitation maximum of BODIPY remains almost unchanged. This allows the BODIPY-DPA dyad to be used as a ratiometric sensor of singlet oxygen.

Keywords: reactive oxygen species; singlet oxygen; sensor; BODIPY; DPA; anthracene

1. Introduction

Reactive oxygen species (ROS) play an essential role in cellular metabolism [1–3] as well as in photodynamic therapy (PDT) of diseases [4–6]. Singlet oxygen ($^1\text{O}_2$) is one of the most important ROS involved in many intracellular processes in normal conditions and in pathology, and it is also actively generated by photosensitizers in PDT [7]. A number of sensors for singlet oxygen detection have now been developed (Figure 1). Colorimetric sensors allow to monitor the $^1\text{O}_2$ level spectrophotometrically. These sensors are based on dyes, whose absorption spectrum changes considerably after binding to singlet oxygen. In organic solvents, 1,3-diphenylisobenzofuran (DPBF) is usually used to monitor the dynamics of $^1\text{O}_2$ generation [8], whereas in aqueous solutions, the water-soluble anthracene derivative 9,10-anthracenediyl-bis(methylene)dimalonic acid (ABDA) is usually used [9]. It was shown that DPBF can react with $^1\text{O}_2$ with high efficiency, but also exhibits activity against other ROS [10], while anthracene derivatives demonstrate extremely high specificity to $^1\text{O}_2$ [11]. To monitor the generation of $^1\text{O}_2$ in living cells, fluorogenic sensors are widely used. Singlet Oxygen Sensor Green (SOSG) is commercially available and is probably the most commonly used one [12–14], but other sensors fluorescing in green (Aarhus Sensor

Green) [15], red (Si-DMA) [16], or blue (Coumarin 120—Anthracene) [17] spectral region are also described. They consist of dyads of anthracene, responsible for $^1\text{O}_2$ binding, and a chromophore capable of fluorescence in the corresponding spectral range. Due to photoelectron transfer (PET) between the anthracene and the chromophore, the dye initially does not fluoresce, but upon binding of $^1\text{O}_2$ to anthracene the chromophore “lights up” (Figure 1). Such sensors are intensimetric, meaning that they enable monitoring the process by the dye fluorescence intensity in a given channel. In contrast, ratiometric sensors allow the determining of target analytes by the ratio of fluorescence signal intensity in different channels [18]. This makes it possible to determine analyte concentrations more precisely. In the case of $^1\text{O}_2$ sensors, the ratio of intensities in different channels can be used to distinguish the termination of the $^1\text{O}_2$ generation process from the termination of a reactive probe. Recently, ratiometric sensors of singlet oxygen based on 1,3-diarylisobenzofurans have been described [19]; however, like DPBF, they should demonstrate side specificity to other ROS.

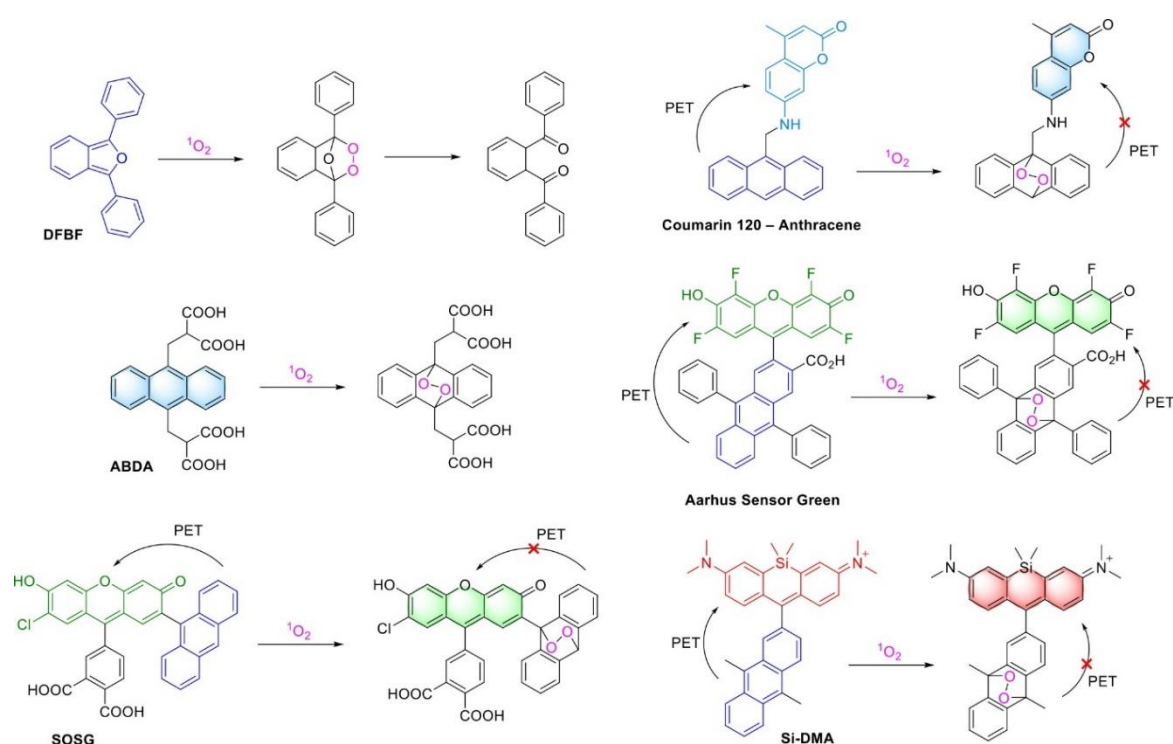


Figure 1. Examples of colorimetric and fluorescent singlet oxygen sensors, as well as reactions leading to changes in its optical properties.

In the present work, we have synthesized a ratiometric sensor of singlet oxygen based on a pair of 9,10-diphenylanthracene (DPA) and 4,4-difluoro-4-bora-3a,4a-diazas-indacene (BODIPY) dyes. Here, DPA acts as a sensitive module, whereas BODIPY acts as a reference dye whose fluorescence is independent of the presence of $^1\text{O}_2$. Thus, the synthesized probe, on the one hand, is ratiometric and, on the other hand, is based on the highly specific $^1\text{O}_2$ anthracene.

BODIPY derivatives have recently become extremely popular for imaging and sensing in living systems [20–23]. They are usually characterized by high fluorescence quantum yield, narrow excitation and emission bands of fluorescence, high photostability, and, perhaps most attractively, they can be readily derivatized to produce dyes with new optical or sensory properties [24–27]. It has been shown that BODIPY derivatives can react with and generate ROS [28–32]. Thus, BODIPY 581/691 can react with $^1\text{O}_2$ through double bonds [33], and a series of SOX sensors can react through furan moieties [34] (Figure 2). However, polyenes and furan derivatives are not highly specific to $^1\text{O}_2$ and readily react

with other ROS [11,35]. Several anthracene-BODIPY conjugates have recently been reported, but they have been used as ROS generators for PDT [36–39].

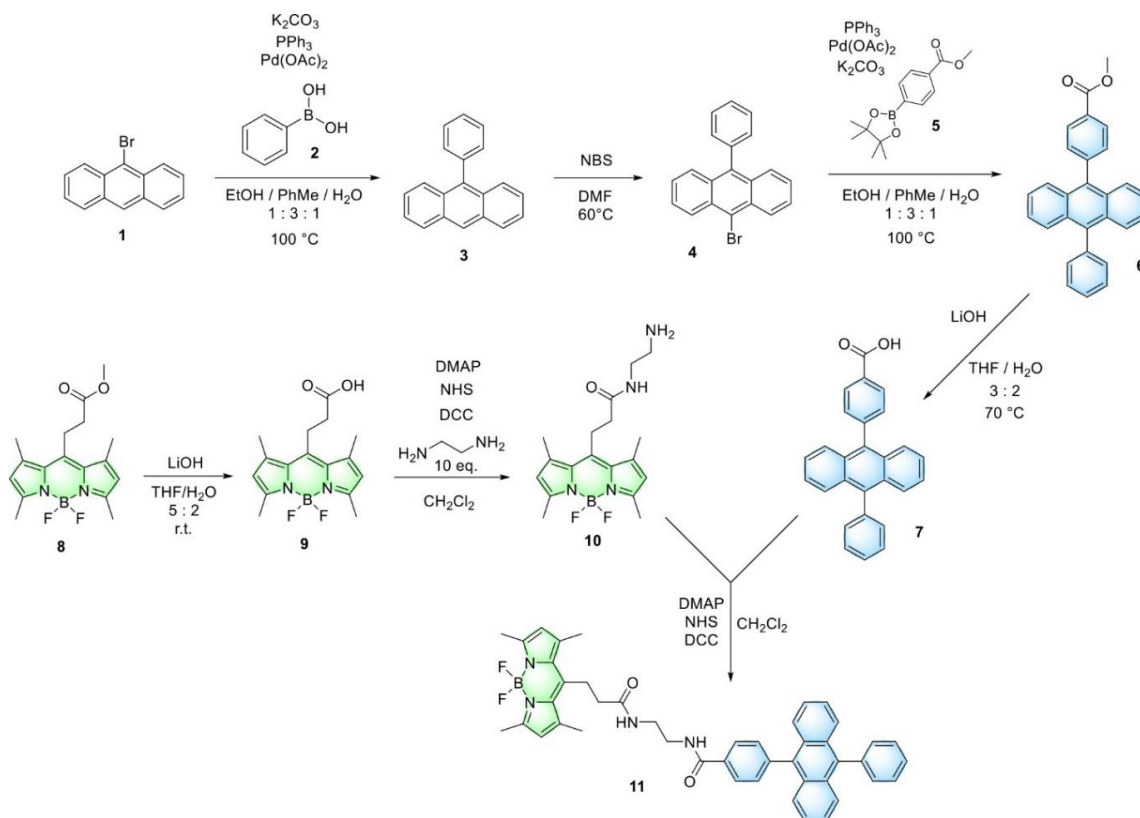


Figure 2. Structures of some BODIPY derivatives that can be used as sensors for $^1\text{O}_2$. ROS binding sites are marked with magenta.

2. Results and Discussion

2.1. Synthesis of BODIPY-DPA Dyad

Dyad, containing BODIPY and DPA fragments in the structure, was prepared from carboxylic derivatives of BODIPY and DPA. Carboxyl-containing 9,10-diphenylanthracene **7** (DPA-COOH) was prepared in several steps according to Scheme 1. BODIPY-COOME **8** and BODIPY-COOH **9** were prepared as described earlier [40]. BODIPY-COOH **9** was reacted with 10-fold excess of ethylenediamine in the presence of DCC, NHS and DMAP to form amino-derivative **10**, which was reacted with DPA-COOH **7** at the same conditions to form BODIPY-DPA dyad **11**. All products were purified by column chromatography on silica. The structure of the synthesized compounds was determined by ^1H , ^{13}C , ^{19}F NMR, IR and MS analysis (Supplementary Materials, Figures S1–S18).



Scheme 1. Synthesis of BODIPY-DPA dyad **11**.

2.2. Optical Properties of the Synthesized Compounds

The optical properties of monomers DPA-COOMe **6** and BODIPY-COOMe **8**, as well as of dyad BODIPY-DPA **11**, were studied in detail in various solvents at room temperature and are presented in Table 1. Normalized electronic absorption and emission spectra of compounds **6**, **8** and **11** are shown in Figure 3 and Figures S19–S22. As seen in Figure 3, the absorption spectra of DPA-COOMe **6** in dichloromethane and toluene consist of practically identical structured bands. The first intense bands, which can be attributed to the S₀→S₁ transition, have several resolved peaks at about 396, 375 (maximum), 357, 340 and 324 nm. The emission spectra of DPA-COOMe **6** consist of one broad peak with maxima at approximately 425 nm in dichloromethane and 421 nm in toluene. The fluorescence quantum yields of DPA-COOMe **6** in dichloromethane and toluene are 0.83 and 0.74, respectively.

Table 1. Photophysical properties of the synthesized compounds.

Compound	Solvent	λ_{abs} (nm)	ϵ (M ⁻¹ cm ⁻¹)	λ_{em} (nm)	Φ_f	Φ_{ET} ⁶	Φ_{ET} ⁷
DPA-COOMe 6	Dichloromethane	375	12,000	425	0.83 ¹		
	Toluene	375	12,000	421	0.74 ¹		
BODIPY-COOMe 8	Dichloromethane	502	78,300	511	0.86 ²		
	Toluene	505	79,100	514	0.95 ²		
DPA-BODIPY 11	Dichloromethane	375 (D)	-	424 (D)	0.76 (B) ³	0.99	0.72
		502 (B)		512 (B)	0.01 (D) ⁴		
	Toluene	375 (D)	-	425 (D)	0.60 (T) ⁵	0.99	0.65
		504 (B)		515 (B)	0.90 (B) ³		

¹ Aerated solution of 9,10-diphenylanthracene in cyclohexane was used as a standard ($\Phi_f = 0.7$)— Φ_{375}^D . ² Solution of fluorescein in 0.1N NaOH was used as a standard ($\Phi_f = 0.91$)— Φ_{475}^{BODIPY} . ³ Emission of BODIPY part (excitation at 475 nm)— Φ_{475}^{BODIPY} . ⁴ Emission of DPA part (excitation at 375 nm)— Φ_{375}^{DA} . ⁵ Total emission (excitation at 375 nm)— $\Phi_{375}^{DA} + \Phi_{375}^{BODIPY}$. ⁶ The energy transfer efficiency was calculated using equation: $\Phi_{ET} = 1 - \Phi_{375}^{DA} / \Phi_{375}^D$. ⁷ The energy transfer efficiency was calculated from dyads quantum yields measured with excitation at 375 nm and 475 nm using equation: $\Phi_{ET} = \frac{\Phi_{375}^{BODIPY} (\epsilon_{375}^{DPA} + \epsilon_{375}^{BODIPY})}{\Phi_{475}^{BODIPY} \epsilon_{375}^{DPA}} - \frac{\epsilon_{375}^{BODIPY}}{\epsilon_{375}^{DPA}}$. Details on this equation can be found in the Supplementary Materials.

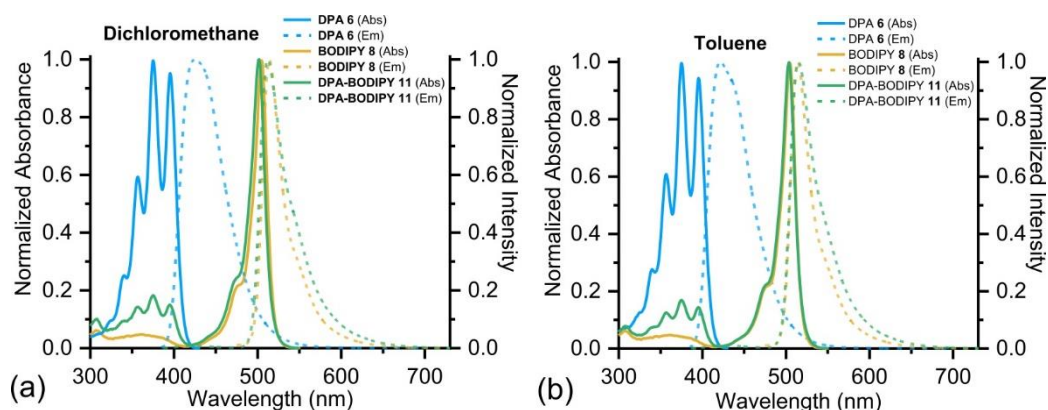


Figure 3. Normalized UV-visible absorption and emission spectra of DPA-COOMe **11**, BODIPY-COOMe **8** and BODIPY-DPA **6** in dichloromethane (a) and toluene (b) at room temperature. Excitation at 375 nm for DPA-COOMe **6**, BODIPY-DPA **11** and at 475 nm for BODIPY-COOMe **8**.

The absorption bands of BODIPY-COOMe **8** in dichloromethane and toluene, which are attributed to the BODIPY S₀→S₁ transition, are sharp and well-resolved, with maxima at 502 nm (in dichloromethane) and 505 nm (in toluene). Fluorescence spectra of BODIPY-COOMe **8** consist of one narrow peak with maxima at 511 nm in dichloromethane and 514 nm in toluene. Fluorescence quantum yields are 0.86 and 0.95 in dichloromethane and toluene, respectively.

The absorption spectra of BODIPY-DPA dyad **11** are close to linear combinations of the absorption spectra of the DPA and BODIPY moieties with the corresponding maxima at about 375 and 500 nm. When BODIPY-DPA **11** is excited at 375 nm, dual emission at wavelengths of about 425 nm (from DPA moiety) and 515 nm (from the BODIPY moiety) are observed. However, it is clearly seen that the fluorescence of DPA is negligible, which can be explained by energy transfer from the excited donor unit (DPA) to the acceptor (BODIPY). The quantum yields of dyad **11** (when excited at 375 nm) and the BODIPY moiety of **11** (when excited at 475 nm) are significant, but somewhat lower than for BODIPY-COOMe **8**, in both solvents (Table 1). Comparison of the shape of the fluorescence spectra of BODIPY-COOMe **8** with BODIPY-DPA **11** indicates its broadening for the dyad **11** that can be attributed to the appearance of a new band corresponding to conformers in which DPA and BODIPY moieties are in close proximity. Analogous spectral behavior was observed for the DBMBF2-BODIPY dyad described earlier [41].

Using the obtained extinction coefficients and quantum yields, we calculated the energy transfer efficiency (Φ_{ET}) from donor to acceptor by two methods (Table 1). According to the method considering only the energy loss by donor, the energy transfer efficiency is 99% (Table 2, Φ_{ET}^6). However, if energy received by acceptor is taken into account the efficiency of energy transfer from the donor to the acceptor is about 70% (Table 2, Φ_{ET}^7). Thus, the additional ways of energy loss by donor, such as conformation rearrangement process should be considered. It has recently been shown that in multichromophore BODIPY compounds, chromophore interactions within the molecule can lead to the formation of different types of aggregates and the appearance of excimer-like states. This significantly affects the optical properties of the compound, including brightness [42]. Importantly, these properties strongly depend on the parameters of the medium in which the dye is located.

Table 2. The results of analysis of fluorescence decay kinetics of compounds **6**, **8** and **11**.

Compound	Solvent	τ (ns) at 431 nm, $\lambda_{ex} = 375$ nm	τ (ns) at 511 nm, $\lambda_{ex} = 375$ nm	τ (ns) at 511 nm, $\lambda_{ex} = 440$ nm	Global Fitting	
					τ (ns), $\lambda_{ex} = 375$ nm	τ (ns), $\lambda_{ex} = 440$ nm
DPA-COOMe 6	Dichloromethane	5.25				
	Toluene	4.57				
BODIPY-COOMe 8	Dichloromethane		5.3	5.34		
	Toluene		4.9	4.94		
DPA-BODIPY 11	Dichloromethane	5.24 (37%)	5.28 (79%)	5.3 (74%)	5.29	5.26
		1.54 (8%)	0.96 (21%)	0.96 (26%)	0.98	0.63
		0.07 (55%)			0.05	
	Toluene	4.8 (3%)	4.96 (84%)	4.93 (74%)	4.92	4.93
		1.74 (7%)	0.80 (16%)	0.74 (26%)	1.27	0.5
		0.06 (90%)			0.06	

For a more detailed analysis of the interchromophore interactions in the DPA-BODIPY dyad, we analyzed the kinetics of fluorescence decays. The fluorescence decay kinetics of compounds **6** and **8** are monoexponential and do not depend on excitation wavelength. The lifetimes are summarized in Table 2. The fluorescence decay of compound **11** measured at 511 nm with excitation at 440 nm when only BODIPY moiety should be excited is biexponential (Figure 4a,b and Table 2). The global fitting of time-resolved fluorescence emission spectra (TRES) obtained with excitation at 440 nm in both toluene and dichloromethane demonstrates the same results (Table 2 and Appendix A, Figure A1). The spectra of amplitudes corresponding to exponential term with lifetime τ_2 (0.63 and 0.5 ns in dichloromethane and toluene, respectively) have negative amplitudes in 530–600 nm range (Figure A1), indicating a conformational rearrangement process. The TRES obtained for solution of **11** in toluene with 375 nm excitation requires a three-exponential model for a satisfactory fit. The same model can be applied to TRES obtained in dichloromethane, but this does not lead to significant improvement in fitting quality (Table 2 and Appendix A, Figure A2). The presence of an additional fast component is clearly seen in Figure 4c,d.

The additional fast component with a lifetime of about 60 ps in toluene and about 50 ps in dichloromethane appears in this case, which apparently can be attributed to energy transfer process.

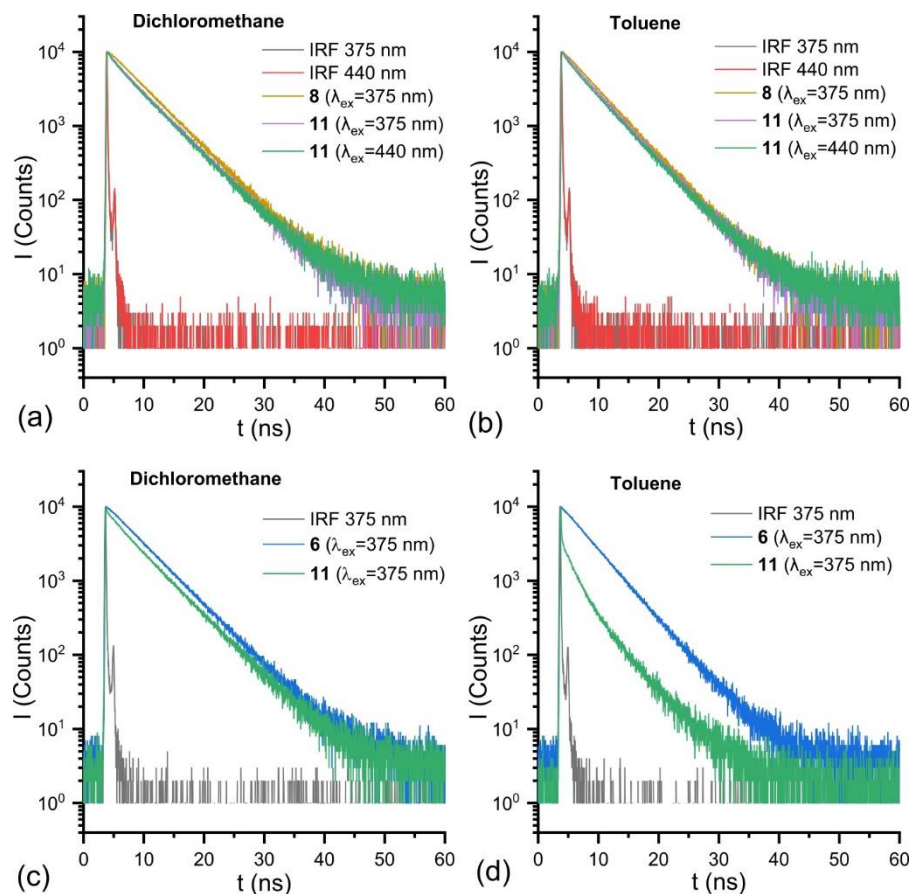


Figure 4. Fluorescence decay kinetics of compound **8** and **11** in dichloromethane (a) and toluene (b) obtained at 511 nm and for compounds **6** and **11** in dichloromethane (c) and toluene (d) measured at 431 nm (excitation wavelengths are written in the corresponding figures).

Thus, the analysis of the optical properties of BODIPY-DPA **11** clearly indicates the presence of interchromophore interactions in ground and excited states. The interactions result in the decrease of fluorescence quantum yield. On the other hand, due to the spatial proximity of the chromophores, there is an energy transfer from the donor to the acceptor, resulting in emission only in the green region. Thus, dyad **11** has two fluorescence excitation peaks, from anthracene and BODIPY, but the emission occurs predominantly from BODIPY.

2.3. Singlet Oxygen Detection

To study the sensitivity of the BODIPY-DPA **11** dyad to singlet oxygen, we used the RoseBengal singlet oxygen generator, which has a maximum absorption at 562 nm and a shoulder at 520 nm (Figure 5a), allowing us to spectrally separate it from BODIPY and DPA. To the RoseBengal solution, BODIPY-DPA **11** was added, the mixture was irradiated with green light, and $^1\text{O}_2$ generation was monitored by changes in the absorption and fluorescence spectra (Figure 5). One can see a decrease of characteristic anthracene absorption peaks in the 320–400 nm region during the reaction (Figure 5a). At the same time, the changes in the absorption region of BODIPY are not so significant. The similar changes are observed in the fluorescence excitation spectra (Figure 5b). In the fluorescence emission spectra when excited at 375 nm (Figure 5c), DPA fluorescence is virtually not observed. In the region of the BODIPY emission, the expected decrease of fluorescence

intensity during the reaction is observed. The fluorescence remains considerable even after the completion of the process, since BODIPY also has an excitation maximum at 375 nm. A slight increase of both absorption and excitation peaks of BODIPY is clearly visible at the beginning of irradiation (Figure 5d,e). This can be attributed to the disruption of the interactions of BODIPY with DPA after the reaction with $^1\text{O}_2$ (Scheme 2). The further decrease in BODIPY absorption could be explained either by photodegradation under the action of green light or by degradation caused by the generated singlet oxygen. In any case, the ratio of fluorescence intensities when excited at 500 nm to 375 nm increases significantly over time (3.3-fold, Figure 5f). Thus, this ratio can be used to monitor the dynamics of singlet oxygen generation.

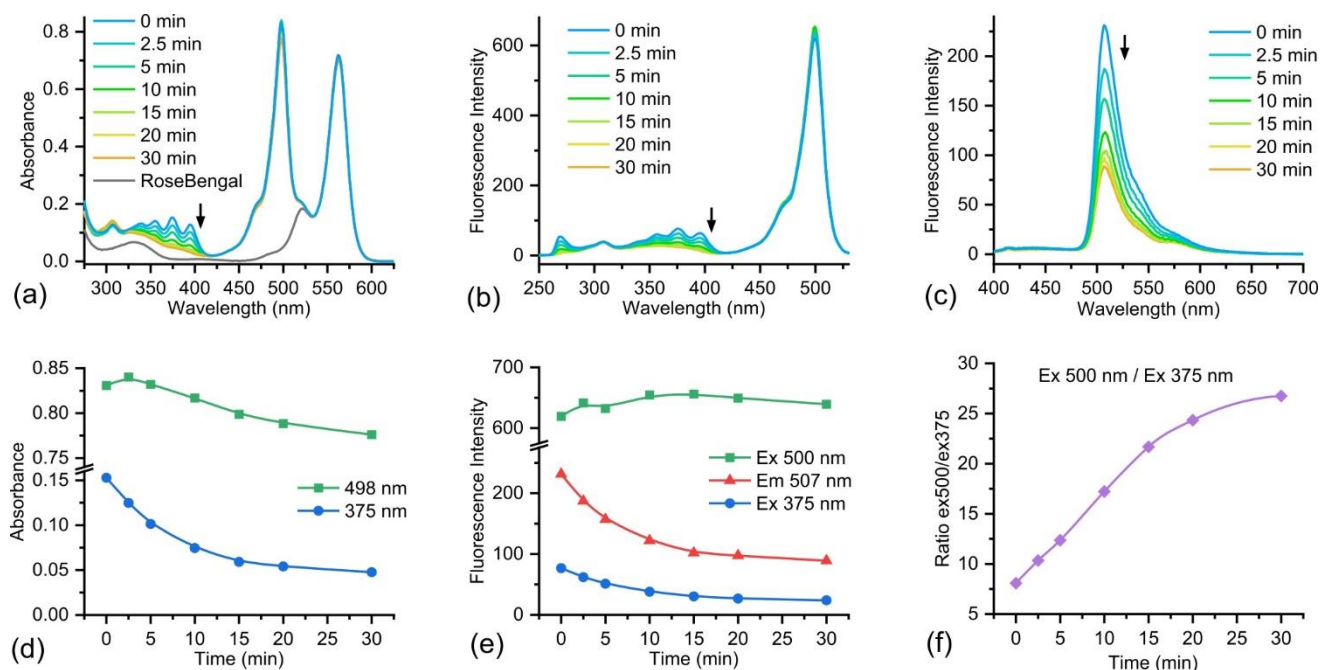
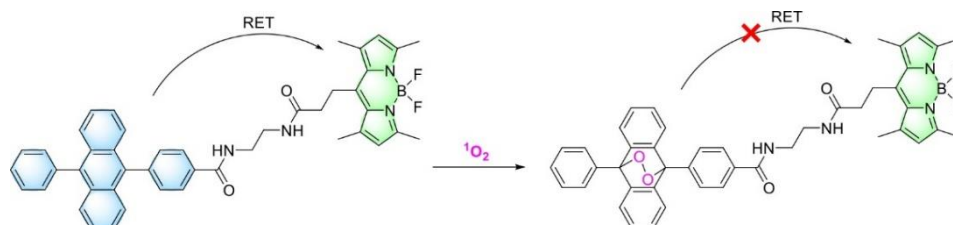


Figure 5. Absorption (a), fluorescence excitation (b), and fluorescence emission (c) spectra of BODIPY-DPA **11** in the course of singlet oxygen generation by RoseBengal. Spectra before and after green light irradiation for 2.5, 5, 10, 15, 20 and 30 min. Dynamics of absorption (d) and fluorescence (e) change at the specified wavelengths, as well as the ratio of fluorescence intensities when excited at 500 nm to 375 nm (f).



Scheme 2. Reaction of BODIPY-DPA **11** with singlet oxygen.

3. Materials and Methods

The experimental details are presented in the Supplementary Materials.

4. Conclusions

In summary, in the present work, a BODIPY-DPA dyad was synthesized. In this dyad, the DPA unit acts as a highly specific oxygen sensor, whereas BODIPY acts as a reference fluorophore. The interchromophoric interactions between DPA and BODIPY lead, on the one hand, to a slight decrease in the fluorescence quantum yield and to the appearance of

components with short fluorescence lifetime. On the other hand, due to the energy transfer from DPA to BODIPY, no DPA emission is observed in the fluorescence spectra; excitation of both DPA and BODIPY results in the fluorescence of the latter. When reacting with singlet oxygen, the intensity of the fluorescence excitation maximum associated with DPA decreases, while the excitation maximum of the BODIPY remains practically unchanged. This allows the BODIPY-DPA dyad to be used as a ratiometric sensor of singlet oxygen.

Supplementary Materials: The following supporting information can be downloaded at: <https://www.mdpi.com/article/10.3390/molecules27249060/s1>.

Author Contributions: Conceptualization, A.A.P. and Y.N.K.; methodology, validation, formal analysis, investigation, A.A.P., A.S.B., A.G.K., Y.N.K., D.S.I., M.A.M. and A.Y.F.; writing—original draft preparation, visualization, writing—review and editing, A.A.P., Y.N.K. and D.S.I.; supervision, project administration, funding acquisition, A.A.P., Y.N.K., D.S.I., M.V.A., V.I.M. and A.M.M. All authors have read and agreed to the published version of the manuscript.

Funding: The synthesis and photophysical characterization of all compounds were supported by the Russian Science Foundation (grant no. 19-73-20194). NMR and IR spectroscopic data were obtained using the equipment of Center for molecule composition studies of INEOS RAS with the financial support from Ministry of Science and Higher Education of the Russian Federation. Fluorescence lifetime measurements were performed using equipment of the Shared Research Center «Structural diagnostics of materials» of FSRC Crystallography and Photonics» RAS and supported by the Ministry of Science and Higher Education within the State assignment FSRC «Crystallography and Photonics» RAS.

Institutional Review Board Statement: Not applicable.

Informed Consent Statement: Not applicable.

Data Availability Statement: Not applicable.

Conflicts of Interest: The authors declare no conflict of interest. The funders had no role in the design of the study; in the collection, analyses, or interpretation of data; in the writing of the manuscript; or in the decision to publish the results.

Appendix A

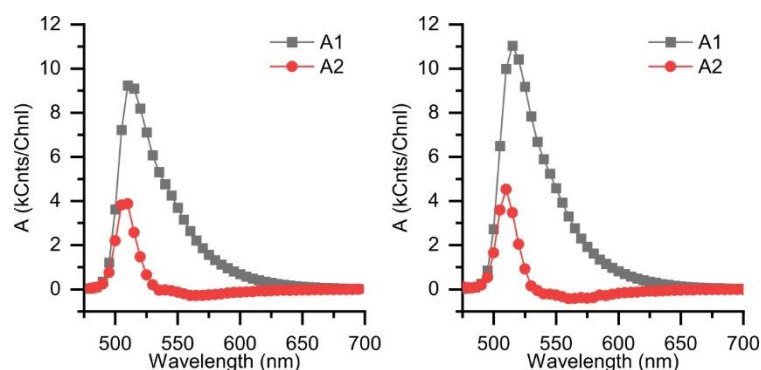


Figure A1. Spectra of amplitudes A_1 , A_2 obtained from global fitting of time-resolved fluorescence spectra of **11** in dichloromethane (**left**) and toluene (**right**) $\lambda_{\text{ex}} = 440$ nm.

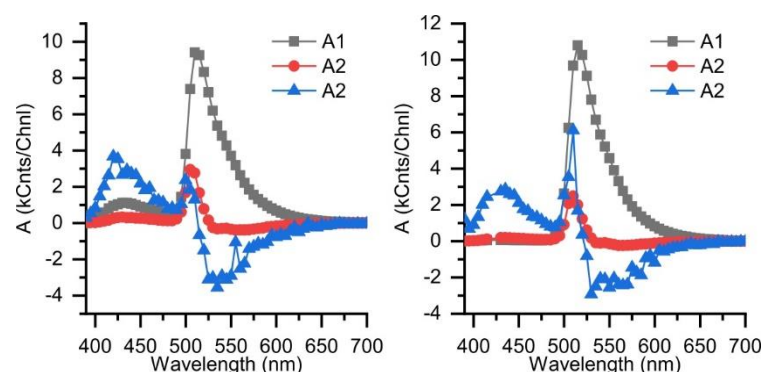


Figure A2. Spectra of amplitudes A_1 – A_3 obtained from global fitting of time-resolved fluorescence spectra of **11** in dichloromethane (**left**) and toluene (**right**) $\lambda_{\text{ex}} = 375$ nm.

References

1. Apel, K.; Hirt, H. Reactive Oxygen Species: Metabolism, Oxidative Stress, and Signal Transduction. *Annu. Rev. Plant Biol.* **2004**, *55*, 373–399. [[CrossRef](#)] [[PubMed](#)]
2. Forrester, S.J.; Kikuchi, D.S.; Hernandez, M.S.; Xu, Q.; Griendling, K.K. Reactive Oxygen Species in Metabolic and Inflammatory Signaling. *Circ. Res.* **2018**, *122*, 877–902. [[CrossRef](#)] [[PubMed](#)]
3. Romo-González, M.; Ijurko, C.; Hernández-Hernández, Á. Reactive Oxygen Species and Metabolism in Leukemia: A Dangerous Liaison. *Front. Immunol.* **2022**, *13*, 889875. [[CrossRef](#)] [[PubMed](#)]
4. Agostinis, P.; Berg, K.; Cengel, K.A.; Foster, T.H.; Girotti, A.W.; Gollnick, S.O.; Hahn, S.M.; Hamblin, M.R.; Juzeniene, A.; Kessel, D.; et al. Photodynamic Therapy of Cancer: An Update. *CA Cancer J. Clin.* **2011**, *61*, 250–281. [[CrossRef](#)]
5. Chilakamarthi, U.; Giribabu, L. Photodynamic Therapy: Past, Present and Future. *Chem. Rec.* **2017**, *17*, 775–802. [[CrossRef](#)]
6. Lan, M.; Zhao, S.; Liu, W.; Lee, C.; Zhang, W.; Wang, P. Photosensitizers for Photodynamic Therapy. *Adv. Healthc. Mater.* **2019**, *8*, 1900132. [[CrossRef](#)]
7. Kashyap, A.; Ramasamy, E.; Ramalingam, V.; Pattabiraman, M. Supramolecular Control of Singlet Oxygen Generation. *Molecules* **2021**, *26*, 2673. [[CrossRef](#)]
8. Gomes, A.; Fernandes, E.; Lima, J.L.F.C. Fluorescence Probes Used for Detection of Reactive Oxygen Species. *J. Biochem. Biophys. Methods* **2005**, *65*, 45–80. [[CrossRef](#)]
9. Krajczewski, J.; Rucińska, K.; Townley, H.E.; Kudelski, A. Role of Various Nanoparticles in Photodynamic Therapy and Detection Methods of Singlet Oxygen. *Photodiagn. Photodyn. Ther.* **2019**, *26*, 162–178. [[CrossRef](#)]
10. Ohyashiki, T.; Nunomura, M.; Katoh, T. Detection of Superoxide Anion Radical in Phospholipid Liposomal Membrane by Fluorescence Quenching Method Using 1,3-Diphenylisobenzofuran. *Biochim. Et Biophys. Acta (BBA)-Biomembr.* **1999**, *1421*, 131–139. [[CrossRef](#)]
11. Entradas, T.; Waldron, S.; Volk, M. The Detection Sensitivity of Commonly Used Singlet Oxygen Probes in Aqueous Environments. *J. Photochem. Photobiol. B Biol.* **2020**, *204*, 111787. [[CrossRef](#)] [[PubMed](#)]
12. Gollmer, A.; Arnbjerg, J.; Blaikie, F.H.; Pedersen, B.W.; Breitenbach, T.; Daasbjerg, K.; Glasius, M.; Ogilby, P.R. Singlet Oxygen Sensor Green[®]: Photochemical Behavior in Solution and in a Mammalian Cell: Photochemistry and Photobiology. *Photochem. Photobiol.* **2011**, *87*, 671–679. [[CrossRef](#)] [[PubMed](#)]
13. Dallas, P.; Velasco, P.Q.; Lebedeva, M.; Porfyakis, K. Detecting the Photosensitization from Fullerenes and Their Dyads with Gold Nanoparticles with Singlet Oxygen Sensor Green. *Chem. Phys. Lett.* **2019**, *730*, 130–137. [[CrossRef](#)]
14. Liu, H.; Carter, P.J.H.; Laan, A.C.; Eelkema, R.; Denkova, A.G. Singlet Oxygen Sensor Green Is Not a Suitable Probe for $^1\text{O}_2$ in the Presence of Ionizing Radiation. *Sci. Rep.* **2019**, *9*, 8393. [[CrossRef](#)] [[PubMed](#)]
15. Pedersen, S.K.; Holmehave, J.; Blaikie, F.H.; Gollmer, A.; Breitenbach, T.; Jensen, H.H.; Ogilby, P.R. Aarhus Sensor Green: A Fluorescent Probe for Singlet Oxygen. *J. Org. Chem.* **2014**, *79*, 3079–3087. [[CrossRef](#)]
16. Kim, S.; Tachikawa, T.; Fujitsuka, M.; Majima, T. Far-Red Fluorescence Probe for Monitoring Singlet Oxygen during Photodynamic Therapy. *J. Am. Chem. Soc.* **2014**, *136*, 11707–11715. [[CrossRef](#)]
17. Sasikumar, D.; Kohara, R.; Takano, Y.; Yuyama, K.; Biju, V. Kinetics of Singlet Oxygen Sensing Using 9-Substituted Anthracene Derivatives. *J. Chem. Sci.* **2019**, *131*, 5. [[CrossRef](#)]
18. Martynov, V.I.; Pakhomov, A.A.; Deyev, I.E.; Petrenko, A.G. Genetically Encoded Fluorescent Indicators for Live Cell PH Imaging. *Biochim. Biophys. Acta (BBA)-Gen. Subj.* **2018**, *1862*, 2924–2939. [[CrossRef](#)]
19. Song, D.; Cho, S.; Han, Y.; You, Y.; Nam, W. Ratiometric Fluorescent Probes for Detection of Intracellular Singlet Oxygen. *Org. Lett.* **2013**, *15*, 3582–3585. [[CrossRef](#)]
20. Martynov, V.I.; Pakhomov, A.A. BODIPY Derivatives as Fluorescent Reporters of Molecular Activities in Living Cells. *Russ. Chem. Rev.* **2021**, *90*, 1213–1262. [[CrossRef](#)]

21. Hwang, T.-Y.; Choi, Y.; Song, Y.; Eom, N.S.A.; Kim, S.; Cho, H.-B.; Myung, N.V.; Choa, Y.-H. A Noble Gas Sensor Platform: Linear Dense Assemblies of Single-Walled Carbon Nanotubes (LACNTs) in a Multi-Layered Ceramic/Metal Electrode System (MLES). *J. Mater. Chem. C* **2018**, *6*, 972–979. [[CrossRef](#)]
22. Cheng, H.; Cao, X.; Zhang, S.; Zhang, K.; Cheng, Y.; Wang, J.; Zhao, J.; Zhou, L.; Liang, X.; Yoon, J. BODIPY as Multifunctional Theranostic Reagent in Biomedicine: Self-Assembly, Properties and Applications. *Adv. Mater.* **2022**, 2207546. [[CrossRef](#)] [[PubMed](#)]
23. Kolemen, S.; Akkaya, E.U. Reaction-Based BODIPY Probes for Selective Bio-Imaging. *Coord. Chem. Rev.* **2018**, *354*, 121–134. [[CrossRef](#)]
24. Loudet, A.; Burgess, K. BODIPY Dyes and Their Derivatives: Syntheses and Spectroscopic Properties. *Chem. Rev.* **2007**, *107*, 4891–4932. [[CrossRef](#)] [[PubMed](#)]
25. Lu, H.; Mack, J.; Yang, Y.; Shen, Z. Structural Modification Strategies for the Rational Design of Red/NIR Region BODIPYs. *Chem. Soc. Rev.* **2014**, *43*, 4778–4823. [[CrossRef](#)] [[PubMed](#)]
26. Poddar, M.; Misra, R. Recent Advances of BODIPY Based Derivatives for Optoelectronic Applications. *Coord. Chem. Rev.* **2020**, *421*, 213462. [[CrossRef](#)]
27. Antina, E.; Bumagina, N.; Marfin, Y.; Guseva, G.; Nikitina, L.; Sbytov, D.; Telegin, F. BODIPY Conjugates as Functional Compounds for Medical Diagnostics and Treatment. *Molecules* **2022**, *27*, 1396. [[CrossRef](#)]
28. Kamkaew, A.; Lim, S.H.; Lee, H.B.; Kiew, L.V.; Chung, L.Y.; Burgess, K. BODIPY Dyes in Photodynamic Therapy. *Chem. Soc. Rev.* **2013**, *42*, 77–88. [[CrossRef](#)]
29. Kue, C.S.; Ng, S.Y.; Voon, S.H.; Kamkaew, A.; Chung, L.Y.; Kiew, L.V.; Lee, H.B. Recent Strategies to Improve Boron Dipyrromethene (BODIPY) for Photodynamic Cancer Therapy: An Updated Review. *Photochem. Photobiol. Sci.* **2018**, *17*, 1691–1708. [[CrossRef](#)]
30. Nguyen, V.-N.; Ha, J.; Cho, M.; Li, H.; Swamy, K.M.K.; Yoon, J. Recent Developments of BODIPY-Based Colorimetric and Fluorescent Probes for the Detection of Reactive Oxygen/Nitrogen Species and Cancer Diagnosis. *Coord. Chem. Rev.* **2021**, *439*, 213936. [[CrossRef](#)]
31. Malacarne, M.C.; Gariboldi, M.B.; Caruso, E. BODIPYs in PDT: A Journey through the Most Interesting Molecules Produced in the Last 10 Years. *Int. J. Mol. Sci.* **2022**, *23*, 10198. [[CrossRef](#)] [[PubMed](#)]
32. Prieto-Montero, R.; Prieto-Castañeda, A.; Sola-Llano, R.; Agarrabeitia, A.R.; García-Fresnadillo, D.; López-Arbeloa, I.; Villanueva, A.; Ortiz, M.J.; Moya, S.; Martínez-Martínez, V. Exploring BODIPY Derivatives as Singlet Oxygen Photosensitizers for PDT. *Photochem. Photobiol.* **2020**, *96*, 458–477. [[CrossRef](#)] [[PubMed](#)]
33. Drummen, G.P.C.; Gadella, B.M.; Post, J.A.; Brouwers, J.F. Mass Spectrometric Characterization of the Oxidation of the Fluorescent Lipid Peroxidation Reporter Molecule C11-BODIPY581/591. *Free. Radic. Biol. Med.* **2004**, *36*, 1635–1644. [[CrossRef](#)] [[PubMed](#)]
34. Kaya, S.; Ismaiel, Y.A.; Kwon, N.; Kim, G.; Bila, J.L.; Yoon, J.; Seven, O.; Akkaya, E.U. Imaging of Intracellular Singlet Oxygen with Bright BODIPY Dyes. *Dye. Pigment.* **2021**, *188*, 109158. [[CrossRef](#)]
35. Laguerre, M.; Lecomte, J.; Villeneuve, P. Evaluation of the Ability of Antioxidants to Counteract Lipid Oxidation: Existing Methods, New Trends and Challenges. *Prog. Lipid Res.* **2007**, *46*, 244–282. [[CrossRef](#)]
36. Zhu, J.; Zou, J.; Zhang, J.; Sun, Y.; Dong, X.; Zhang, Q. An Anthracene Functionalized BODIPY Derivative with Singlet Oxygen Storage Ability for Photothermal and Continuous Photodynamic Synergistic Therapy. *J. Mater. Chem. B* **2019**, *7*, 3303–3309. [[CrossRef](#)]
37. Mahmood, Z.; Taddei, M.; Rehmat, N.; Bussotti, L.; Doria, S.; Guan, Q.; Ji, S.; Zhao, J.; Di Donato, M.; Huo, Y.; et al. Color-Tunable Delayed Fluorescence and Efficient Spin–Orbit Charge Transfer Intersystem Crossing in Compact Carbazole-Anthracene-Bodipy Triads Employing the Sequential Electron Transfer Approach. *J. Phys. Chem. C* **2020**, *124*, 5944–5957. [[CrossRef](#)]
38. Callaghan, S.; Filatov, M.A.; Savoie, H.; Boyle, R.W.; Senge, M.O. In Vitro Cytotoxicity of a Library of BODIPY-Anthracene and -Pyrene Dyads for Application in Photodynamic Therapy. *Photochem. Photobiol. Sci.* **2019**, *18*, 495–504. [[CrossRef](#)]
39. Callaghan, S.; Vindstad, B.E.; Flanagan, K.J.; Melø, T.B.; Lindgren, M.; Grenstad, K.; Gederaas, O.A.; Senge, M.O. Structural, Photophysical, and Photobiological Studies on BODIPY-Anthracene Dyads. *ChemPhotoChem* **2021**, *5*, 131–141. [[CrossRef](#)]
40. Pakhomov, A.A.; Kononevich, Y.N.; Stukalova, M.V.; Svidchenko, E.A.; Surin, N.M.; Cherkaev, G.V.; Shchegolikhina, O.I.; Martynov, V.I.; Muzafarov, A.M. Synthesis and Photophysical Properties of a New BODIPY-Based Siloxane Dye. *Tetrahedron Lett.* **2016**, *57*, 979–982. [[CrossRef](#)]
41. Kononevich, Y.N.; Belova, A.S.; Ionov, D.S.; Sazhnikov, V.A.; Pakhomov, A.A.; Alifimov, M.V.; Muzafarov, A.M. Novel DBMBF 2-BODIPY Dyads Connected via a Flexible Linker: Synthesis and Photophysical Properties. *New J. Chem.* **2022**, *46*, 12739–12750. [[CrossRef](#)]
42. Pakhomov, A.A.; Kim, E.E.; Kononevich, Y.N.; Ionov, D.S.; Maksimova, M.A.; Khalchenia, V.B.; Maksimov, E.G.; Anisimov, A.A.; Shchegolikhina, O.I.; Martynov, V.I.; et al. Modulation of the Photophysical Properties of Multi-BODIPY-Siloxane Conjugates by Varying the Number of Fluorophores. *Dye. Pigment.* **2022**, *203*, 110371. [[CrossRef](#)]